Identification of the thermo-physical properties of a stratified tissue. Adiabatic hypodermic wall

M. Alosaimi[1,2], D. Lesnic[1,*] and J. Niesen[1]

[1]*Department of Applied Mathematics, University of Leeds, Leeds LS2 9JT, UK*
[2]*Department of Mathematics, Taif University, Taif P.O. Box 888, Saudi Arabia*
E-mails: mmmaal@leeds.ac.uk (M. Alosaimi), amt5ld@maths.leeds.ac.uk (D. Lesnic*
corresponding author), j.niesen@leeds.ac.uk (J. Niesen)

Abstract. Biological living tissues possess thermophysical properties that are difficult to measure directly and their estimation is very important in order to decide the appropriate treatment procedure (e.g. place of inoculation and appropriate amount of drug dosage) in case an abnormality is detected. In the present paper, we numerically investigate, for the first time, the determination of several thermo-physical blood-tissue properties of a one-dimensional, multi-layered biological skin tissue subjected to external heating. In contrast to the usual parabolic model that assumes infinitely fast propagation of the heat signal, in the present paper, the bio-heat transfer in such a biological body is mathematically modelled by a hyperbolic partial differential equation, which takes into account that the thermal wave speed is finite. On the skin surface a convective boundary condition holds taking into account the heat exchange with the environment, whilst on the most inner wall of the tissue an adiabatic boundary condition applies. Then, in this framework, the piecewise constant thermo-physical properties of interest given by the thermal conductivity, heat capacity and blood perfusion rate are accurately and stably reconstructed from non-intrusive temperature measurements on the inner and outer boundaries of the multi-layered tissue by minimizing a weighted nonlinear least-squares objective function.

Keywords Inverse problem; thermal-wave model; bio-heat transfer; multi-layered tissue

1. Introduction

Biological tissues such as the skin are prone to be affected/damaged by thermal hazard, e.g. burns (contact or scald), flash fire or laser irradiations [1, 16, 24]. Not only in these thermal exposures but also in cancer detection [19, 20], general thermal damage [15] and in the determination of the thermal dose in hyperthermia treatments [12], several mathematical models for bio-heat conduction have been successfully formulated and increasingly utilized, e.g. the Pennes' bio-heat parabolic model [21] and the thermal-wave hyperbolic model [11]. Panda and Das [19, 20] proposed an inversion mechanism for detecting the presence/absence of cancer in biological tissues by estimating some of its biological features. Similar to these works, the papers [6, 22] considered the bio-heat parabolic model and utilized genetic algorithms and the Markov Chain Monte Carlo method, respectively, for cancer detection purposes. Narasimhan and Sadasivam [15] gained insights into the evaluation of retinal damage occurred in medical treatment of ocular disorders by employing a hyperbolic-type bio-heat conduction model subsequently used to compute the Arrhenius damage integral, whereas Loulou and Scott [12] utilized an inverse methodology based on the bio-heat parabolic model to optimize the thermal dose required for the destruction of tumours.

As far as inverse bio-heat transfer problems are concerned, a substantial amount of research has been carried out based on the Pennes' bio-heat parabolic model or concerned

with single-layered tissues. For instance, Baghban and Ayani [2] estimated the intensity of external heating applied to treat an abnormal triple-layered skin tissue by using a sequential method, whereas Yue et al. [29] estimated the thermal conductivity, heat capacity and blood perfusion rate of a cylindrical single-layered probe from non-invasive surface temperature measurements. Besides, Panda and Das [20] considered the thermal-wave hyperbolic model and proposed a differential evolution algorithm to recover non-invasively the blood perfusion rate in a 1-D single-layered biological body from its surface temperature measurement. Lee et al. [9] utilized the thermal-wave hyperbolic model and the conjugate gradient method (CGM) to reconstruct the heat flux at a 1-D one-layered tissue's surface.

Numerical methods have been powerful tools, enabling discretisation of the above mathematical models along with the prescribed initial and boundary conditions. These include the finite-difference method (FDM) [19, 20], the finite element/volume methods [17] and the boundary element method [3, 25]. Furthermore, to complement these methods devised for the numerical solution of direct problems, various additional optimization methods have to be designed and applied for inversion, e.g. the golden section search method (GSSM) [19], genetic algorithms [6], the CGM [9] and the nonlinear Tikhonov regularization method [26].

Prior to this work, the above studies either neglected the relaxation time observed in biological bodies and accounted for by the thermal-wave hyperbolic model, or they did not consider stratified tissues. The former assumption is required to reflect the microstructure of real tissues of the human bodies, e.g. three layers [1], four layers [27], or seven layers [15], as in skin, thigh or eye, respectively. In addition of taking into account for these extra practically realistic features, the novelty of the current work also consists of, for the first time, the recovery of the thermal conductivity, heat capacity and blood perfusion rate of a typical triple-layered skin tissue formed of the epidermis, dermis and hypodermis (or subcutaneous) layers, as illustrated in Figure 1. In summary, the novelty of the communication consists in altogether:

(i) taking into account for the finite speed of heat propagation in biological tissues which generalizes the parabolic Pennes equation into the more realistic hyperbolic thermal-wave equation;

(ii) considering the multi-layered material consisting of the epidermis, dermis and hypodermis instead of the single layer model;

(iii) determining the thermal properties (thermal conductivity, heat capacity and blood perfusion rate) for each layer from non-intrusive boundary temperature measurements only using a Matlab toolbox routine based on the trust-region reflective algorithm.

The article is structured as follows. In Section 2, the governing model of thermal-wave bio-heat transfer in multi-layered biological tissues is formulated. In Section 3, the direct problem concerning a one-dimensional, triple-layered skin tissue subjected to a laser aggression is numerically solved using the FDM. Section 4 describes the numerical inversion procedure subsequently used for the retrieval of the thermo-physical properties of interest. Results of the inversion of both exact and noisy data are presented and discussed. Conclusions are highlighted in Section 5.

2. Mathematical formulation

The partial differential equation (PDE) governing the heat propagation in biological tissues, which takes into account that the thermal wave speed is not infinite, is described by the
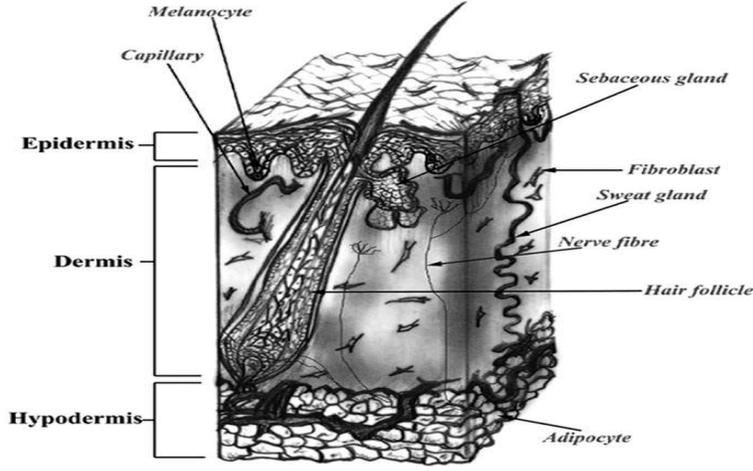
Figure 1: Triple-layered skin tissue [7].

hyperbolic equation [11]:

$$\rho_t c_t \tau \frac{\partial^2 T}{\partial t^2} + (\rho_t c_t + \tau w_b \rho_b c_b)\frac{\partial T}{\partial t} = k\nabla^2 T + w_b \rho_b c_b(T_a - T) + Q_m + Q_e + \tau\frac{\partial}{\partial t}(Q_m + Q_e),$$
$$\text{in } \Omega \times (0, t_f], \quad (1)$$

where Ω represents the tissue domain, $t_f > 0$ denotes the duration of the transient process, T, ρ_t, c_t and k are the temperature [K], density [kg/m³], specific heat [Joule/(kg K)] and thermal conductivity [W/(m K)] of the tissue, respectively, ρ_b, c_b and w_b are the density [kg/m³], specific heat [Joule/(kg K)] and perfusion rate [s^{-1}] of the blood, respectively, τ is the relaxation time [s], ∇^2 is the Laplace operator, t is the time [s] and T_a is the (arterial) blood temperature [K]. Furthermore, Q_e and Q_m are the external and metabolic heats [W/m³]. Also, we denote by $\alpha = k/(\rho_t c_t)$ the tissue's thermal diffusivity [m²/s]. Equation (1) has been derived by modifying the parabolic Pennes' bio-heat reaction-diffusion equation to include the finite speed (equal to $\sqrt{\alpha/\tau}$) of energy propagation present in biological tissues through the non-negligible relaxation time τ in between 15-30 s. This gives rise to the generalized Fourier's law expressing the heat flux $q(x,t)$ as:

$$-k\nabla T(x,t) = q(x, t+\tau) \approx q(x,t) + \tau\frac{\partial q}{\partial t}(x,t), \quad (x,t) \in \Omega \times (0, t_f]. \quad (2)$$

It it interesting to note that the zero-flux condition $q(x,t) \cdot n(x) = 0$ on $\partial\Omega \times (0, t_f]$, where n is the outward unit normal to the boundary $\partial\Omega$, maintains as the zero-Neumann boundary condition $-k\partial_n T = 0$, but a non-zero flux prescription does not maintain its usual form in terms of the normal derivative of T, [28]. On the other hand the invariance holds for a Robin boundary condition that arises from a generalized Newton's law of the form, [14],

$$\left(q(x,t) + \tau\frac{\partial q}{\partial t}(x,t)\right) \cdot n(x) = -h(T_\infty - T(x,t)) \quad \text{on } \partial\Omega \times (0, t_f], \quad (3)$$

where h represents the heat transfer coefficient [W/(m² K)] and T_∞ is the ambient temperature [K]. Then, assuming that (2) holds at the boundary we obtain the usual Newton's law boundary condition, [8],

$$k\nabla T(x,t) \cdot n(x) = h(T_\infty - T(x,t)), \quad (x,t) \in \partial\Omega \times (0, t_f]. \quad (4)$$

3

Assuming that the tissue Ω is a one-dimensional composite material formed of J disjoint layers $[L_{l-1}, L_l]$ for $l = \overline{1, \mathrm{J}}$, equation (1) transforms into [10]:

$$C_{\mathrm{t}}^l \tau_l \frac{\partial^2 T_l}{\partial t^2} + \left(C_{\mathrm{t}}^l + \tau_l w_b^l C_b\right) \frac{\partial T_l}{\partial t} = k_l \frac{\partial^2 T_l}{\partial x^2} + w_b^l C_b (T_a - T_l) + Q_m^l + Q_e^l + \tau_l \frac{\partial}{\partial t}(Q_m^l + Q_e^l),$$
$$(x, t) \in [L_{l-1}, L_l] \times (0, t_{\mathrm{f}}], \quad l = \overline{1, \mathrm{J}}, \quad (5)$$

with the corresponding thermo-physical properties annotated by the super/sub-script l for each layer, and $C_{\mathrm{t}}^l = \rho_{\mathrm{t}}^l c_{\mathrm{t}}^l$ [Joule/(m^3 K)] and $C_b = \rho_b c_b$ [Joule/(m^3 K)] denoting the heat capacity of the layer l and blood, respectively.

The above equations are coupled through the usual continuity of the temperature at the interfaces, namely,

$$T_l(L_l, t) = T_{l+1}(L_l, t), \quad t \in [0, t_{\mathrm{f}}], \quad l = \overline{1, (\mathrm{J} - 1)}, \quad (6)$$

and of the heat flux. This latter condition needs to be considered more carefully since in the case of the Maxwell-Cattaneo equation (1) (or (5)), the heat flux is given by the generalized Fourier's law (2). Then, on imposing the continuity of the heat flux at the interface $q_l(L_l, t) = q_{l+1}(L_l, t)$ we also have that $\frac{\partial q_l}{\partial t}(L_l, t) = \frac{\partial q_{l+1}}{\partial t}(L_l, t)$ and equation (2) implies that:

$$k_l \frac{\partial T_l}{\partial x}(L_l, t) = k_{l+1} \frac{\partial T_{l+1}}{\partial x}(L_l, t), \quad t \in [0, t_{\mathrm{f}}], \quad l = \overline{1, (\mathrm{J} - 1)}, \quad (7)$$

provided that $\tau_l = \tau_{l+1}$ for all $l = \overline{1, (\mathrm{J} - 1)}$, i.e. the relaxation time is the same constant $\tau > 0$ over each layer, which we shall assume from now on.

For the hyperbolic PDE (5), we assume that the initial temperature is uniform and equal to a constant T_0 while the heating process is initiated from rest, in which case the initial conditions are given by:

$$T_l(x, 0) = T_0, \quad \frac{\partial T_l}{\partial t}(x, 0) = 0, \quad x \in [L_{l-1}, L_l], \quad l = \overline{1, \mathrm{J}}. \quad (8)$$

The upstream end of the tissue $x = L_0$ representing the skin surface is assumed in contact with the ambient air, while the downstream end $x = L_{\mathrm{J}}$ is assumed insulated (i.e. adiabatic wall), such that the boundary conditions are given by:

$$-k_1 \frac{\partial T_1}{\partial x}(L_0, t) = h\left(T_\infty - T_1(L_0, t)\right), \quad \frac{\partial T_{\mathrm{J}}}{\partial x}(L_{\mathrm{J}}, t) = 0, \quad t \in [0, t_{\mathrm{f}}]. \quad (9)$$

The above adiabatic wall boundary condition, which assumes that the heat flux approaches zero deep in tissue at $x = L_{\mathrm{J}}$, is also realistic for biological body, [10].

We further assume that the metabolic heat is neglected, i.e. $Q_m^l = 0$ for $l = \overline{1, \mathrm{J}}$, and that the external heating is due to a laser irradiation of the form, [1],

$$Q_e^l(x, t) = \mu I_0 H(t_{\mathrm{p}} - t) e^{-\mu x}, \quad (x, t) \in [L_{l-1}, L_l] \times (0, t_{\mathrm{f}}], \quad l = \overline{1, \mathrm{J}}, \quad (10)$$

where μ is the extinction coefficient of the tissue [m^{-1}], I_0 denotes the power of laser [W/m^2], t_{p} represents the laser irradiation's duration [s] and H is the Heaviside step function. The

Heaviside step function H appearing in (10) is approximated using the hyperbolic tangent function as:

$$H(t_\mathrm{p} - t) \approx \frac{1}{2}\left(1 + \tanh\left(\frac{50(t_\mathrm{p} - t)}{t_\mathrm{f}}\right)\right), \quad t \in (0, t_\mathrm{f}]. \tag{11}$$

2.1 Dimensionless model
First, in order to avoid a discontinuity at the origin $(0, 0)$, the compatibility between the initial temperature condition (8) and the Robin boundary condition (9) requires that $T_\infty = T_0$. We can then non-dimensionalize the thermal-wave model of the previous section by introducing new dimensionless variables defined by:

$$(\bar{x}, \mathrm{L}_l) = \frac{(x, L_l)}{L_\mathrm{J}}, \qquad (\bar{t}, t_\mathrm{p}) = \frac{(t, t_\mathrm{p})}{t_\mathrm{f}}, \qquad \theta_l = \frac{T_l - T_0}{T_0}. \tag{12}$$

Then, the dimensionless version of the governing equation (5)-(9) (removing the bars on x and t for clarity) can be expressed as:

$$\frac{\partial^2 \theta_l}{\partial t^2} + a_1^l \frac{\partial \theta_l}{\partial t} = a_2^l \frac{\partial^2 \theta_l}{\partial x^2} - a_3^l \left(\theta_l + \frac{T_0 - T_a}{T_0}\right)$$

$$+ \frac{a_4^l}{2}\left(1 + \tanh\left(50\left(t_\mathrm{p} - t\right)\right) - \frac{50\tau}{t_\mathrm{f}}\mathrm{sech}^2\left(50\left(t_\mathrm{p} - t\right)\right)\right)e^{-\mu x L_\mathrm{J}},$$

$$(x, t) \in [\mathrm{L}_{l-1}, \mathrm{L}_l] \times (0, 1], \quad l = \overline{1, \mathrm{J}}, \tag{13}$$

$$\theta_l\Big|_{t=0} = 0, \quad \frac{\partial \theta_l}{\partial t}\Big|_{t=0} = 0 \quad \text{in } [\mathrm{L}_{l-1}, \mathrm{L}_l], \quad l = \overline{1, \mathrm{J}}, \tag{14}$$

$$\begin{aligned}\theta_l(\mathrm{L}_l, t) &= \theta_{l+1}(\mathrm{L}_l, t), & t &\in [0, 1], & l &= \overline{1, (\mathrm{J} - 1)}, \\ a_5^l \frac{\partial \theta_l}{\partial x}(\mathrm{L}_l, t) &= \frac{\partial \theta_{l+1}}{\partial x}(\mathrm{L}_l, t), & t &\in [0, 1], & l &= \overline{1, (\mathrm{J} - 1)},\end{aligned} \tag{15}$$

$$a_6 \frac{\partial \theta_1}{\partial x}(\mathrm{L}_0, t) = \theta_1(\mathrm{L}_0, t), \quad \frac{\partial \theta_\mathrm{J}}{\partial x}(1, t) = 0, \quad t \in [0, 1], \tag{16}$$

where:

$$a_1^l = \frac{t_\mathrm{f}}{\tau} + \frac{w_b^l C_b t_\mathrm{f}}{C_\mathrm{t}^l}, \quad a_2^l = \frac{k_l t_\mathrm{f}^2}{\tau C_\mathrm{t}^l L_\mathrm{J}^2}, \quad a_3^l = \frac{t_\mathrm{f}}{\tau}\left(a_1^l - \frac{t_\mathrm{f}}{\tau}\right), \quad a_4^l = \frac{\mu I_0 t_\mathrm{f}^2}{\tau T_0 C_\mathrm{t}^l}, \quad l = \overline{1, \mathrm{J}},$$

$$a_5^l = \frac{a_2^l a_4^{l+1}}{a_4^l a_2^{l+1}}, \quad l = \overline{1, (\mathrm{J} - 1)}, \quad a_6 = \frac{\mu I_0 L_\mathrm{J} a_2^1}{h T_0 a_4^1}. \tag{17}$$

The inversion of (17) yields back the dimensional variables given by:

$$C_\mathrm{t}^l = \frac{\mu I_0 t_\mathrm{f}^2}{\tau T_0 a_4^l}, \quad k_l = \frac{\tau C_\mathrm{t}^l L_\mathrm{J}^2 a_2^l}{t_\mathrm{f}^2}, \quad w_b^l = \frac{C_\mathrm{t}^l}{C_b t_\mathrm{f}}\left(a_1^l - \frac{t_\mathrm{f}}{\tau}\right), \quad l = \overline{1, \mathrm{J}}. \tag{18}$$

3. Numerical solution of direct problem
Denoting $Q^l := [\mathrm{L}_{l-1}, \mathrm{L}_l] \times (0, 1]$ for $l = \overline{1, \mathrm{J}}$, we consider the more general hyperbolic direct problem associated to (13)-(16) given by:

$$\frac{\partial^2 u_l}{\partial t^2} + b_l \frac{\partial u_l}{\partial t} = c_l \frac{\partial^2 u_l}{\partial x^2} - d_l u_l + f_l \quad \text{in } Q^l, \tag{19}$$

5

where b_l, c_l and d_l are known positive constants, and f_l are known functions for $l = \overline{1, \mathrm{J}}$,

$$u_l\Big|_{t=0} = \phi_l, \quad \frac{\partial u_l}{\partial t}\Big|_{t=0} = \psi_l \quad \text{in } [\mathrm{L}_{l-1}, \mathrm{L}_l], \tag{20}$$

where ϕ_l and ψ_l are prescribed functions for $l = \overline{1, \mathrm{J}}$,

$$
\begin{aligned}
u_l(\mathrm{L}_l, t) &= u_{l+1}(\mathrm{L}_l, t), & t &\in [0, 1], \\
\gamma_l \frac{\partial u_l}{\partial x}(\mathrm{L}_l, t) &= \frac{\partial u_{l+1}}{\partial x}(\mathrm{L}_l, t), & t &\in [0, 1],
\end{aligned}
\tag{21}
$$

where γ_l are prescribed positive constants for $l = \overline{1, (\mathrm{J} - 1)}$, and

$$u_1(\mathrm{L}_0, t) + \beta \frac{\partial u_1}{\partial x}(\mathrm{L}_0, t) = R(t), \qquad \frac{\partial u_{\mathrm{J}}}{\partial x}(\mathrm{L}_{\mathrm{J}}, t) = 0, \quad t \in [0, 1], \tag{22}$$

where $\mathrm{L}_{\mathrm{J}} = 1$, $\beta \neq 0$ is a prescribed constant and $R(t)$ is a prescribed function.

Introducing the intermediate variable v_l, [5], as:

$$v_l := \frac{\partial u_l}{\partial t} + b_l u_l \quad \text{in } Q^l, \quad l = \overline{1, \mathrm{J}}, \tag{23}$$

then equation (19) recasts as

$$\frac{\partial v_l}{\partial t} = c_l \frac{\partial^2 u_l}{\partial x^2} - d_l u_l + f_l \quad \text{in } Q^l, \quad l = \overline{1, \mathrm{J}}. \tag{24}$$

From (20) and (23),

$$v_l\Big|_{t=0} = \psi_l + b_l \phi_l \quad \text{in } [\mathrm{L}_{l-1}, \mathrm{L}_l], \quad l = \overline{1, \mathrm{J}}. \tag{25}$$

We subdivide the computational domain Q^l into M^l and N uniform meshes $\Delta x_l = (\mathrm{L}_l - \mathrm{L}_{l-1})/M^l$ and $\Delta t = 1/N$, respectively. We let $P_0 = 0$ and $P_l = \sum_{r=1}^{l} M^r$ for $l = \overline{1, \mathrm{J}}$.

Denote $u_{i,j}^l := u_l(x_i, t_j)$, $v_{i,j}^l := v_l(x_i, t_j)$, $\left(u_{i,j}^l\right)_x := \frac{\partial u_l}{\partial x}(x_i, t_j)$ and $f_{i,j}^l := f_l(x_i, t_j)$, where $x_i = \mathrm{L}_{l-1} + (i - P_{l-1})\Delta x_l$, $t_j = j\Delta t$ for $i = \overline{P_{l-1}, P_l}$, $j = \overline{0, N}$.

The FDM discretizes (23), (24), (20), (25), (21) and (22) as:

$$\frac{u_{i,j+1}^l - u_{i,j}^l}{\Delta t} = \frac{1}{2}\left(v_{i,j}^l - b_l u_{i,j}^l + v_{i,j+1}^l - b_l u_{i,j+1}^l\right), \tag{26}$$

$$\frac{v_{i,j+1}^l - v_{i,j}^l}{\Delta t} = \frac{1}{2}\left(\frac{c_l}{(\Delta x_l)^2}\delta_x^2 u_{i,j}^l - d_l u_{i,j}^l + f_{i,j}^l + \frac{c_l}{(\Delta x_l)^2}\delta_x^2 u_{i,j+1}^l - d_l u_{i,j+1}^l + f_{i,j+1}^l\right), \tag{27}$$

$$i = \overline{(P_{l-1} + 1), (P_l - 1)}, \quad j = \overline{0, (N-1)}, \quad l = \overline{1, \mathrm{J}},$$

$$\frac{v_{i,j+1}^l - v_{i,j}^l}{\Delta t} = \frac{1}{2}\left(\frac{2c_l}{(\Delta x_l)^2}\tilde{\delta}_x^2 u_{i,j}^l - d_l u_{i,j}^l + f_{i,j}^l + \frac{2c_l}{(\Delta x_l)^2}\tilde{\delta}_x^2 u_{i,j+1}^l - d_l u_{i,j+1}^l + f_{i,j+1}^l\right), \tag{28}$$

$$i = P_{l-1}, \quad j = \overline{0, (N-1)}, \quad l = \overline{1, \mathrm{J}},$$

$$\frac{v_{i,j+1}^l - v_{i,j}^l}{\Delta t} = \frac{1}{2}\left(\frac{2c_l}{(\Delta x_l)^2}\bar{\delta}_x^2 u_{i,j}^l - d_l u_{i,j}^l + f_{i,j}^l + \frac{2c_l}{(\Delta x_l)^2}\bar{\delta}_x^2 u_{i,j+1}^l - d_l u_{i,j+1}^l + f_{i,j+1}^l\right), \tag{29}$$

6

$$i = P_l, \quad j = \overline{0, (N-1)}, \quad l = \overline{1, \mathrm{J}},$$

$$u_{i,0}^l = \phi_l(x_i), \quad v_{i,0}^l = \psi_l(x_i) + b_l\phi_l(x_i), \quad i = \overline{P_{l-1}, P_l}, \quad l = \overline{1, \mathrm{J}}, \tag{30}$$

$$u_{P_l,j}^l = u_{P_l,j}^{l+1}, \quad \gamma_l\left(u_{P_l,j}^l\right)_x = \left(u_{P_l,j}^{l+1}\right)_x, \quad j = \overline{0, N}, \quad l = \overline{1, (\mathrm{J}-1)}, \tag{31}$$

$$u_{0,j}^1 + \beta\left(u_{0,j}^1\right)_x = R(t_j), \quad \left(u_{P_\mathrm{J},j}^\mathrm{J}\right)_x = 0, \quad j = \overline{0, N}, \tag{32}$$

where $\delta_x^2 u_{i,j}^l = u_{i-1,j}^l - 2u_{i,j}^l + u_{i+1,j}^l$, $\tilde{\delta}_x^2 u_{i,j}^l = u_{i+1,j}^l - u_{i,j}^l - \Delta x_l\left(u_{i,j}^l\right)_x$ and $\bar{\delta}_x^2 u_{i,j}^l = u_{i-1,j}^l - u_{i,j}^l + \Delta x_l\left(u_{i,j}^l\right)_x$ for $j = \overline{0, N}$. Solving (26) for $v_{i,j+1}^l$, we obtain:

$$v_{i,j+1}^l = \left(b_l + \frac{2}{\Delta t}\right)u_{i,j+1}^l + \left(b_l - \frac{2}{\Delta t}\right)u_{i,j}^l - v_{i,j}^l. \tag{33}$$

Introducing (33) in (27), we obtain:

$$-A_l u_{i-1,j+1}^l + B_l u_{i,j+1}^l - A_l u_{i+1,j+1}^l = A_l u_{i-1,j}^l + C_l u_{i,j}^l + A_l u_{i+1,j}^l + 2v_{i,j}^l$$
$$+ \frac{\Delta t}{2}\left(f_{i,j}^l + f_{i,j+1}^l\right), \tag{34}$$

where $i = \overline{(P_{l-1}+1), (P_l-1)}$, $j = \overline{0, (N-1)}$, $l = \overline{1, \mathrm{J}}$, $A_l = \frac{c_l \Delta t}{2(\Delta x_l)^2}$, $B_l = \left(\frac{2}{\Delta t} + b_l\right) + \frac{c_l \Delta t}{(\Delta x_l)^2} + \frac{d_l \Delta t}{2}$ and $C_l = \left(\frac{2}{\Delta t} - b_l\right) - \left(\frac{c_l \Delta t}{(\Delta x_l)^2} + \frac{d_l \Delta t}{2}\right)$.

Similarly, introducing (33) in (28), we obtain:

$$2\Delta x_{l+1} A_{l+1}\left(u_{P_l,j+1}^{l+1}\right)_x + B_{l+1}u_{P_l,j+1}^{l+1} - 2A_{l+1}u_{P_l+1,j+1}^{l+1} = -2\Delta x_{l+1}A_{l+1}\left(u_{P_l,j}^{l+1}\right)_x + C_{l+1}u_{P_l,j}^{l+1}$$
$$+ 2A_{l+1}u_{P_l+1,j}^{l+1} + 2v_{P_l,j}^{l+1} + \frac{\Delta t}{2}\left(f_{P_l,j}^{l+1} + f_{P_l,j+1}^{l+1}\right), \tag{35}$$

for $j = \overline{0, (N-1)}$, $l = \overline{0, (\mathrm{J}-1)}$, and in (29), we obtain:

$$-2A_l u_{P_l-1,j+1}^l + B_l u_{P_l,j+1}^l - 2\Delta x_l A_l\left(u_{P_l,j+1}^l\right)_x = 2A_l u_{P_l-1,j}^l + C_l u_{P_l,j}^l + 2\Delta x_l A_l\left(u_{P_l,j}^l\right)_x$$
$$+ 2v_{P_l,j}^l + \frac{\Delta t}{2}\left(f_{P_l,j}^l + f_{P_l,j+1}^l\right), \tag{36}$$

for $j = \overline{0, (N-1)}$, $l = \overline{1, \mathrm{J}}$. From (32), the difference equation (35) for $l = 0$ becomes

$$(B_1 - \lambda)u_{0,j+1}^1 - 2A_1 u_{1,j+1}^1 = (C_1 + \lambda)u_{0,j}^1 + 2A_1 u_{1,j}^1 + 2v_{0,j}^1 + \frac{\Delta t}{2}\left(f_{0,j}^1 + f_{0,j+1}^1\right)$$
$$- \lambda\left(R(t_j) + R(t_{j+1})\right), \tag{37}$$

where $\lambda = 2A_1\Delta x_1/\beta$, and the difference equation (36) for $l = \mathrm{J}$ becomes

$$-2A_\mathrm{J} u_{P_\mathrm{J}-1,j+1}^\mathrm{J} + B_\mathrm{J} u_{P_\mathrm{J},j+1}^\mathrm{J} = 2A_\mathrm{J} u_{P_\mathrm{J}-1,j}^\mathrm{J} + C_\mathrm{J} u_{P_\mathrm{J},j}^\mathrm{J} + 2v_{P_\mathrm{J},j}^\mathrm{J} + \frac{\Delta t}{2}\left(f_{P_\mathrm{J},j}^\mathrm{J} + f_{P_\mathrm{J},j+1}^\mathrm{J}\right). \tag{38}$$

For $j = \overline{0, (N-1)}$, $l = \overline{1, (\mathrm{J}-1)}$, multiplying equations (35) and (36) by $\bar{\eta}_l := \Delta x_l A_l$ and by $\tilde{\eta}_l := \gamma_l \Delta x_{l+1} A_{l+1}$, respectively, summing the resulting equations and then using the continuity conditions given by (31), we obtain:

$$-\tilde{A}_l u_{P_l-1,j+1}^l + \tilde{B}_l u_{P_l,j+1}^l - \bar{A}_{l+1} u_{P_l+1,j+1}^{l+1} = \tilde{A}_l u_{P_l-1,j}^l + \tilde{C}_l u_{P_l,j}^l + \bar{A}_{l+1} u_{P_l+1,j}^{l+1}$$

$$+ 2(\tilde{\eta}_l v^l_{P_l,j} + \bar{\eta}_l v^{l+1}_{P_l,j}) + \frac{\Delta t}{2}\big(\tilde{\eta}_l(f^l_{P_l,j} + f^l_{P_l,j+1}) + \bar{\eta}_l(f^{l+1}_{P_l,j} + f^{l+1}_{P_l,j+1})\big), \qquad (39)$$

where $\tilde{A}_l = 2\tilde{\eta}_l A_l$, $\bar{A}_{l+1} = 2\bar{\eta}_l A_{l+1}$, $\tilde{B}_l = \tilde{\eta}_l B_l + \bar{\eta}_l B_{l+1}$ and $\tilde{C}_l = \tilde{\eta}_l C_l + \bar{\eta}_l C_{l+1}$.

At each time step t_{j+1} for $j = \overline{0, (N-1)}$, equations (33), (34), (37), (38) and (39) can be rewritten as:

$$\tilde{L}\tilde{\boldsymbol{u}}_{j+1} = \tilde{E}\tilde{\boldsymbol{u}}_j + 2\tilde{\boldsymbol{v}}_j + \tilde{\boldsymbol{b}}^j, \qquad (40)$$

$$\boldsymbol{v}^l_{j+1} = \left(b_l + \frac{2}{\Delta t}\right)\boldsymbol{u}^l_{j+1} + \left(b_l - \frac{2}{\Delta t}\right)\boldsymbol{u}^l_j - \boldsymbol{v}^l_j, \quad l = \overline{1, \mathrm{J}}, \qquad (41)$$

where:

$$\boldsymbol{u}^l_j = (u^l_{P_{l-1},j}, \ldots, u^l_{P_l,j})^\mathrm{T}, \qquad \boldsymbol{v}^l_j = (v^l_{P_{l-1},j}, \ldots, v^l_{P_l,j})^\mathrm{T}, \qquad \tilde{\boldsymbol{u}}_j = (u^1_{0,j}, \ldots, u^\mathrm{J}_{P_\mathrm{J},j})^\mathrm{T},$$

$$\tilde{\boldsymbol{v}}_j = (v^1_{0,j}, \ldots, \tilde{\eta}_1 v^1_{P_1,j} + \bar{\eta}_1 v^2_{P_1,j}, v^2_{P_1+1,j}, \ldots, \tilde{\eta}_{\mathrm{J}-1} v^{\mathrm{J}-1}_{P_{\mathrm{J}-1},j} + \bar{\eta}_{\mathrm{J}-1} v^\mathrm{J}_{P_{\mathrm{J}-1},j}, v^\mathrm{J}_{P_{\mathrm{J}-1}+1,j}, \ldots, v^\mathrm{J}_{P_\mathrm{J},j})^\mathrm{T},$$

$$\tilde{L} = \begin{pmatrix}
B_1 - \lambda & -2A_1 & & & & & & & & \\
-A_1 & B_1 & -A_1 & & & & & & & \\
& \ddots & \ddots & \ddots & & & & & & \\
& & -\tilde{A}_1 & \tilde{B}_1 & -\bar{A}_2 & & & & & \\
& & & -A_2 & B_2 & -A_2 & & & & \\
& & & & \ddots & \ddots & \ddots & & & \\
& & & & & -\tilde{A}_{\mathrm{J}-1} & \tilde{B}_{\mathrm{J}-1} & -\bar{A}_\mathrm{J} & & \\
& & & & & & -A_\mathrm{J} & B_\mathrm{J} & -A_\mathrm{J} & \\
& & & & & & & \ddots & \ddots & \ddots \\
& & & & & & & & -2A_\mathrm{J} & B_\mathrm{J}
\end{pmatrix},$$

$$\tilde{E} = \begin{pmatrix}
C_1 + \lambda & 2A_1 & & & & & & & & \\
A_1 & C_1 & A_1 & & & & & & & \\
& \ddots & \ddots & \ddots & & & & & & \\
& & \tilde{A}_1 & \tilde{C}_1 & \bar{A}_2 & & & & & \\
& & & A_2 & C_2 & A_2 & & & & \\
& & & & \ddots & \ddots & \ddots & & & \\
& & & & & \tilde{A}_{\mathrm{J}-1} & \tilde{C}_{\mathrm{J}-1} & \bar{A}_\mathrm{J} & & \\
& & & & & & A_\mathrm{J} & C_\mathrm{J} & A_\mathrm{J} & \\
& & & & & & & \ddots & \ddots & \ddots \\
& & & & & & & & 2A_\mathrm{J} & C_\mathrm{J}
\end{pmatrix},$$

$$\tilde{\boldsymbol{b}}^j = \begin{pmatrix} \frac{\Delta t}{2}\left(f_{0,j}^1 + f_{0,j+1}^1\right) - \lambda\left(R(t_j) + R(t_{j+1})\right) \\ \frac{\Delta t}{2}\left(f_{1,j}^1 + f_{1,j+1}^1\right) \\ \vdots \\ \frac{\Delta t}{2}\left(\tilde{\eta}_1\left(f_{P_1,j}^1 + f_{P_1,j+1}^1\right) + \bar{\eta}_1\left(f_{P_1,j}^2 + f_{P_1,j+1}^2\right)\right) \\ \frac{\Delta t}{2}\left(f_{P_1+1,j}^2 + f_{P_1+1,j+1}^2\right) \\ \vdots \\ \frac{\Delta t}{2}\left(\tilde{\eta}_{J-1}\left(f_{P_{J-1},j}^{J-1} + f_{P_{J-1},j+1}^{J-1}\right) + \bar{\eta}_{J-1}\left(f_{P_{J-1},j}^J + f_{P_{J-1},j+1}^J\right)\right) \\ \frac{\Delta t}{2}\left(f_{P_{J-1}+1,j}^J + f_{P_{J-1}+1,j+1}^J\right) \\ \vdots \\ \frac{\Delta t}{2}\left(f_{P_J,j}^J + f_{P_J,j+1}^J\right) \end{pmatrix}.$$

It has been shown elsewhere [23] that the above finite-difference scheme is convergent and unconditionally stable. Moreover, the order of convergence in the L_∞-norm is two in both space and time.

3.1 Direct problem

The physical problem considered herein is concerned with a 1-D triple-layered skin tissue subjected to a short-time laser aggression given by (10) with $\mu = 700$ m^{-1}, $I_0 = 130 \times 10^3$ W/m^2 and $t_{\mathrm{p}} = 1$ s, [1]. The thermo-physical characteristics of the tissue layers presented in Table 1 are taken from [1]. Other parameters are taken from the same reference as: $C_b = 3.9962 \times 10^6$ Joule/(m^3 K), $h = 10$ W/(m^2 K) and $T_a = T_0 = T_\infty = 306$ K. Further, we take $\tau = 20$ s from [18] and $t_{\mathrm{f}} = 40$ s.

Table 1: Properties of a three-layered skin tissue model [1]. Note that 1 W = 1 Joule/s.

	Epidermis $(L_1 - L_0)$	Dermis $(L_2 - L_1)$	Hypodermis $(L_3 - L_2)$	Unit
Thickness	6×10^{-4}	1.4×10^{-3}	2×10^{-3}	m
k	0.235	0.425	0.185	W/(m K)
C_{t}	3.96×10^6	3.65×10^6	2.80×10^6	Joule/(m^3 K)
w_b	0	9.6592×10^{-4}	0	s^{-1}

To verify the FDM described in Section 3, we solve the dimensionless model (13)-(16) using various $N = M^l \in \{40, 60, 80\}$ for $l = 1, 2, 3$ with J = 3 and the above input, which, via (12) and (17), yields

$$a_1^1 = a_1^3 = 2, a_1^2 = 2.0423, a_2^1 = 0.2967, a_2^2 = 0.5822, a_2^3 = 0.3304, a_3^1 = a_3^3 = 0,$$
$$a_3^2 = 0.0846, a_4^1 = 6.0078, a_4^2 = 6.5180, a_4^3 = 8.4967, a_5^1 = 0.5529, a_5^2 = 2.2973, \qquad (42)$$
$$a_6 = 5.875, \mathrm{t_p} = 0.05, \mathrm{L_0} = 0, \mathrm{L_1} = 0.15, \mathrm{L_2} = 0.5, \mathrm{L_3} = 1.$$

Figure 2 depicts numerical realizations of the dimensionless temperature at the boundaries of the tissue. From this figure, it can be clearly observed that the numerical solution for the

tissue temperature is convergent with undistinguishable curves being obtained for various mesh sizes employed. Although the spatial heating radiates according to the short-time laser aggression (10), the negative non-dimensional temperature in Figure 2 indicates, see (12) with $T_0 = T_\infty$, that the actual dimensional boundary temperatures $T_1(0, t)$ and $T_3(0.004, t)$ are lower than the ambient temperature $T_\infty = 306$ K. This is due to the hyperbolic model of bio-heat transfer given by equation (1), in which the negativeness of the time derivative $\frac{\partial Q_e^l}{\partial t}(x, t)$ makes the free term in equation (13) to act as a sink rather than a source if the relaxation time $\tau > 0$ is taken into account.
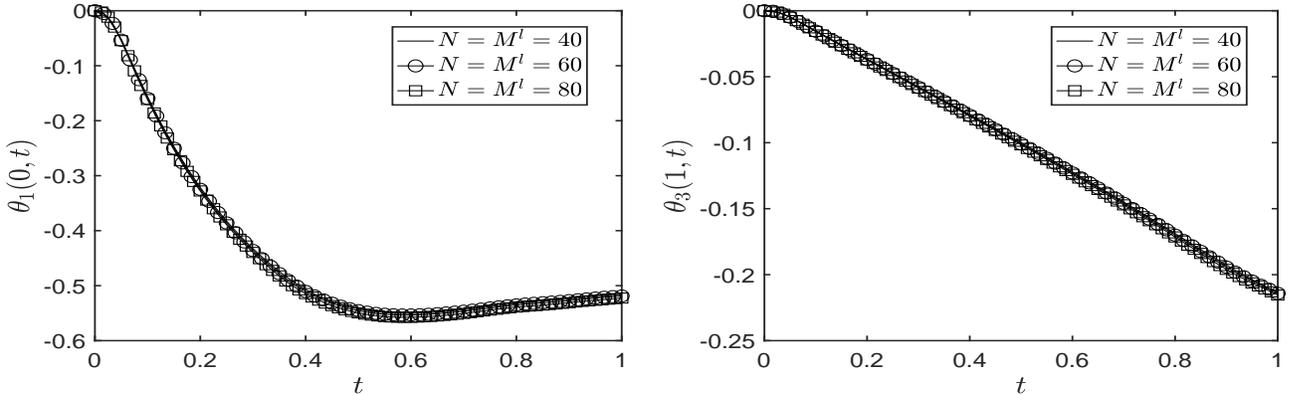

Figure 2: Numerical solutions for $\theta_1(0, t)$ and $\theta_3(1, t)$, for various $N = M^l \in \{40, 60, 80\}$ for $l = 1, 2, 3$, for the direct problem.

4. Numerical solution of inverse problem

The thermo-physical properties $\left(k_l, C_t^l, w_b^l\right)_{l=\overline{1,J}}$ of the dimensional model (5)-(9) are reconstructed from the algebraic expressions (18) which analytically connect them to the dimensionless parameters $\boldsymbol{a} := \left(a_1^l, a_2^l, a_4^l\right)_{l=\overline{1,J}}$ of the governing hyperbolic equation (13)-(16). The latter dimensionless quantities are recovered from temperature measurements at $x \in \{0, 1\}$ by minimizing a weighted least-squares objective function. Such nonlinear minimization problem is solved by utilizing the MATLAB subroutine *lsqnonlin*, [13], based on the trust-region reflective algorithm [4]. The lower and upper bounds for $\left(a_1^l\right)_{l=\overline{1,J}}$ are specified as t_f/τ and 10^3, respectively, and for $\left(a_2^l\right)_{l=\overline{1,J}}$ and $\left(a_4^l\right)_{l=\overline{1,J}}$ are specified as 10^{-3} and 10^3, respectively. Moreover, the initial guess for $\left(a_1^l\right)_{l=\overline{1,J}}$ is taken to be $1.5 t_f/\tau$, and for $\left(a_2^l\right)_{l=\overline{1,J}}$ and $\left(a_4^l\right)_{l=\overline{1,J}}$ to be 0.5.

In the inversion below, we consider the numerically simulated dimensionless boundary temperatures at $x \in \{0, 1\}$ obtained with $N = M^l = 640$ for $l = \overline{1, J}$ from the FDM direct solver as input data and solve the inverse problem with a coarser mesh of $N_{\text{inv}} = M_{\text{inv}}^l = 320$ for $l = \overline{1, J}$. Furthermore, as practical measurements are prone to noise, random noise is added to the numerically simulated data as:

$$\theta_1^\epsilon(0, t_j) = \theta_1(0, t_j) + \epsilon 1_j, \quad \theta_J^\epsilon(1, t_j) = \theta_J(1, t_j) + \epsilon 2_j, \quad j = \overline{1, N_{\text{inv}}}, \tag{43}$$

where $\epsilon 1_j$ and $\epsilon 2_j$ are sampled from a Gaussian normal distribution with zero mean and standard deviations $\sigma_1 = p \times \max_{j=\overline{1,N_{\text{inv}}}} |\theta_1(0, t_j)|$ and $\sigma_2 = p \times \max_{j=\overline{1,N_{\text{inv}}}} |\theta_J(1, t_j)|$, where p stands for the percentage of noise.

To evaluate the accuracy of the reconstructed parameters, the relative error (RE%) is used,

as defined by:

$$\text{RE}(\zeta) = \frac{|\zeta^{\text{numerical}} - \zeta^{\text{exact}}|}{|\zeta^{\text{exact}}|} \times 100\%, \tag{44}$$

where $\zeta^{\text{numerical}}$ stands for the numerically reconstructed value and ζ^{exact} denotes the exact value of the parameter of interest, if available.

4.1 Inverse problem

As previously mentioned, we minimize the objective function given by:

$$G(\boldsymbol{a}) = \frac{1}{\sigma_1^2} \sum_{j=1}^{N_{\text{inv}}} \left(\theta_1(0, t_j) - \theta_1^c(0, t_j; \boldsymbol{a})\right)^2 + \frac{1}{\sigma_2^2} \sum_{j=1}^{N_{\text{inv}}} \left(\theta_3(1, t_j) - \theta_3^c(1, t_j; \boldsymbol{a})\right)^2, \tag{45}$$

where $\theta_1^c(0, t_j; \boldsymbol{a})$ and $\theta_3^c(1, t_j; \boldsymbol{a})$ for $j = \overline{1, N_{\text{inv}}}$ denote the computed boundaryt temperatures at $x \in \{0, 1\}$, (in the case of no noise, i.e. $p = 0$, we take $\sigma_1 = \sigma_2 = 1$).
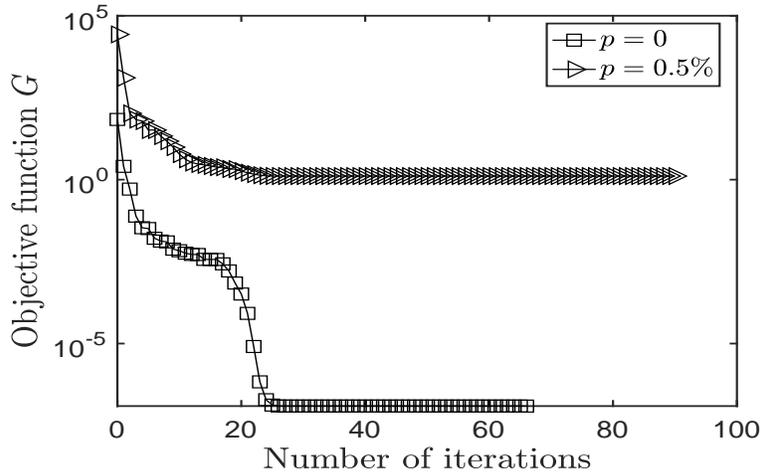

Figure 3: Convergence of the cost function G given by (45).

Figure 3 depicts the convergence of the cost function G given by (45), as a function of the number of iterations, for $p \in \{0, 0.5\%\}$ noise. Table 2 shows the numerical reconstructions of the unknown quantities $\left(a_1^l, a_2^l, a_4^l\right)_{l=1,2,3}$, for $p \in \{0, 0.5\%\}$, along with the exact values for comparison. Table 2 also includes information such as the values of the cost function G given by (45), the number of iterations and the computational time. From this table, it can be concluded that the accuracy and stability of reconstruction of the unknown parameters $\left(a_1^l, a_2^l, a_4^l\right)_{l=1,2,3}$ have been successfully accomplished for noiseless and noisy (for up to $p = 0.5\%$ noise) data.

Finally, the values of $\left(k_l, C_{\text{t}}^l, w_b^l\right)_{l=1,2,3}$ are obtained from the formulae (18), and they are presented in Table 3. From this table, it can be seen that accuracy and stability of the reconstructed values of the quantities $\left(k_l, C_{\text{t}}^l, w_b^l\right)_{l=1,2,3}$ are successfully achieved for $p \in \{0, 0.5\%\}$ noise. Regarding higher percentages of noise such as $p = 1\%$, some relative errors (RE%) of the identified dimensional parameters were found to be of around 10% and thus these results are not presented.

5. Conclusions

The simultaneous reconstruction of several thermo-physical blood-tissue properties of a one-dimensional, triple-layered biological tissue subjected to a laser aggression have been investigated. Such accurate and stable recovery has been obtained by minimizing a weighted

Table 2: Identified dimensionless parameters $\left(a_1^l, a_2^l, a_4^l\right)_{l=1,2,3}$, for $p \in \{0, 0.5\%\}$ noise.

	Exact	$p=0$		$p=0.5\%$	
		Numerical	RE (%)	Numerical	RE (%)
a_1^1	2	2.0008	0.04	2.0024	0.12
a_1^2	2.0426	2.0425	0.01	2.0436	0.06
a_1^3	2	2.0009	0.05	2.0065	0.33
a_2^1	0.2967	0.2971	0.13	0.2997	0.99
a_2^2	0.5822	0.5831	0.16	0.5986	2.82
a_2^3	0.3304	0.3309	0.15	0.3342	1.15
a_4^1	6.0078	6.0120	0.07	6.0148	0.12
a_4^2	6.5180	6.5264	0.13	6.5828	0.99
a_4^3	8.4967	8.5001	0.04	8.4901	0.08
G		1.2383×10^{-7}		1.2859	
Number of iterations		66		90	
Computational time		34 s		42 s	
Criterion for halting iterations		current step has norm less than step tolerance, 10^{-20}		function evaluation limit, 900, is exceeded	

Table 3: Identified thermo-physical properties $\left(k_l, C_t^l, w_b^l\right)_{l=1,2,3}$, for $p \in \{0, 0.5\%\}$ noise.

	Exact	$p=0$		$p=0.5\%$	
		Numerical	RE (%)	Numerical	RE (%)
k_1	0.235	0.2351	0.06	0.2371	0.88
k_2	0.425	0.4251	0.03	0.4327	1.81
k_3	0.185	0.1852	0.11	0.1873	1.23
C_t^1	3.96×10^6	3.9572×10^6	0.07	3.9554×10^6	0.12
C_t^2	3.65×10^6	3.6453×10^6	0.13	3.6141×10^6	0.98
C_t^3	2.80×10^6	2.7989×10^6	0.04	2.8022×10^6	0.08
w_b^1	0	1.9982×10^{-5}	—	5.8163×10^{-5}	—
w_b^2	9.6592×10^{-4}	9.7094×10^{-4}	0.52	9.8580×10^{-4}	2.06
w_b^3	0	1.6131×10^{-5}	—	1.1455×10^{-4}	—

nonlinear least-squares objective function using a numerical procedure that couples an unconditionally stable FDM to the MATLAB optimization toolbox routine *lsqnonlin*.

The adiabatic boundary condition at the hypodermic end $x = L_3$ that has been considered in (9) permitted the associated boundary temperature measurement to be considered. This extra information would not have been possible in case of a Dirichlet boundary condition for which internal measurements of the temperature in the epidermis, dermis or hypodermis might be necessary. The case of the Dirichlet boundary temperature specification at $x = L_3$ is currently under investigation. Also, the present study was concerned with the identification of constant thermo-physical properties, but further work will account for temperature-dependent thermo-physical properties [27].

12

the United Kingdom Saudi Arabian Cultural Bureau (UKSACB) in London for supporting his PhD studies at the University of Leeds.

References

[1] L. Autrique, C. Lormel, Numerical design of experiment for sensitivity analysis–application to skin burn injury prediction, IEEE Trans. Biomed. Eng. 55 (4) (2008) 1279–1290.

[2] M. Baghban, M.B. Ayani, Source term prediction in a multilayer tissue during hyperthermia, J. Therm. Biol. 52 (2015) 187–191.

[3] C.L. Chan, Boundary element method analysis for the bioheat transfer equation, J. Biomech. Eng.-Trans. ASME 114 (3) (1992) 358–365.

[4] T.F. Coleman, Y. Li, An interior trust region approach for nonlinear minimization subject to bounds, SIAM J. Optim. 6 (2) (1996) 418–445.

[5] W. Dai, R. Nassar, A finite difference scheme for solving the heat transport equation at the microscale, Numer. Meth. Part Differ. Equ. 15 (6) (1999) 697–708.

[6] K. Das, S.C. Mishra, Estimation of tumor characteristics in a breast tissue with known skin surface temperature, J. Therm. Biol. 38 (6) (2013) 311–317.

[7] S.R. Edmondson, S.P. Thumiger, G.A. Werther, C.J. Wraight, Epidermal homeostasis: the role of the growth hormone and insulin-like growth factor systems, Endocr. Rev. 24 (6) (2003) 737–764.

[8] M.G. Hennessy, M. Calvo-Schwarzwälder, T.G. Myers, Modelling ultra-fast nanoparticle melting with the Maxwell–Cattaneo equation, Appl. Math. Model. 69 (2019) 201–222.

[9] H.-L. Lee, T.-H. Lai, W.-L. Chen, Y.-C. Yang, An inverse hyperbolic heat conduction problem in estimating surface heat flux of a living skin tissue, Appl. Math. Model. 37 (5) (2013) 2630–2643.

[10] J. Liu, X. Chen, L.X. Xu, New thermal wave aspects on burn evaluation of skin subjected to instantaneous heating, IEEE Trans. Biomed. Eng. 46 (4) (1999) 420–428.

[11] J. Liu, Z. Ren, C. Wang, Interpretation of living tissue's temperature oscillations by thermal wave theory, Chin. Sci. Bull. 40 (17) (1995) 1493–1495.

[12] T. Loulou, E.P. Scott, Thermal dose optimization in hyperthermia treatments by using the conjugate gradient method, Numer. Heat Tranf. A-Appl. 42 (7) (2002) 661–683.

[13] Mathworks (2012) Documentation optimization toolbox-least squares (model fitting) algorithms, available at: www.mathworks.com/help/toolbox/optim/ug/brnoybu.html.

[14] M.J. Maurer, H.A. Thompson, Non-Fourier effects at high heat flux, J. Heat Transf.-Trans. ASME 95 (2) (1973) 284–286.

[15] A. Narasimhan, S. Sadasivam, Non-Fourier bio heat transfer modelling of thermal damage during retinal laser irradiation, Int. J. Heat Mass Transf. 60 (2013) 591–597.

[16] E.Y.K. Ng, L.T. Chua, Mesh-independent prediction of skin burns injury, J. Med. Eng. Technol. 24 (6) (2000) 255–261.

[17] S. Nóbrega, P.J. Coelho, A parametric study of thermal therapy of skin tissue, J. Therm. Biol. 63 (2017) 92–103.

[18] Ş. Özen, S. Helhel, O. Çerezci, Heat analysis of biological tissue exposed to microwave by using thermal wave model of bio-heat transfer (TWMBT), Burns 34 (1) (2008) 45–49.

[19] S. Panda, R. Das, A golden section search method for the identification of skin subsurface abnormalities, Inverse Probl. Sci. Eng. 26 (2) (2018) 183–202.

[20] S. Panda, R. Das, Parameter estimation in a biological system using differential evolution algorithm, 2018 Eleventh International Conference on Contemporary Computing (IC3), IEEE, Noida, 2018, pp. 18263042.

[21] H.H. Pennes, Analysis of tissue and arterial blood temperatures in the resting human forearm, J. Appl. Physiol. 1 (2) (1948) 93–122.

[22] M. Rojczyk, H.R.B. Orlande, M.J. Colaço, I. Szczygieł, A.J. Nowak, R.A. Białecki, Z. Ostrowski, Inverse heat transfer problems: an application to bioheat transfer, Comput. Assist. Meth. Eng. Sci. 22 (4) (2015) 365–383.

[23] H. Sun, Z-.Z. Sun, W. Dai, A second-order finite difference scheme for solving the dual-phase-lagging equation in a double-layered nanoscale thin film, Numer. Meth. Part Differ. Equ. 33 (1) (2017) 142–173.

[24] D.A. Torvi, J.D. Dale, A finite element model of skin subjected to a flash fire, J. Biomech. Eng.-Trans. ASME 116 (3) (1994) 250–255.

[25] D. Trucu, D.B. Ingham, D. Lesnic, Direct boundary element method for the transient bio-heat transfer equation, in: J. Trevelyan (Ed.), Advances in Boundary Integral Methods - Proceedings of the Sixth UK Conference on Boundary Integral Methods, Durham University, Durham, 2007, pp. 223–232.

[26] D. Trucu, D.B. Ingham, D. Lesnic, The inverse coefficient identification problem in bio-heat transient flow equation, in: G.S. Dulikravich, M.J. Colaco, H.R.B. Orlande and M. Tanaka (Eds.), Inverse Problems, Design and Optimization (IPDO-2007), Taylor & Francis, Florida, 2007, pp. 214–221.

[27] M. Tunç, Ü. Çamdali, C. Parmaksizoğlu, S. Çikrikçi, The bio-heat transfer equation and its applications in hyperthermia treatments, Eng. Comput. 23 (4) (2006) 451–463.

[28] Y.J. Yu, Analytical solutions to hyperbolic heat conductive models using Green's function method, J. Therm. Sci. Technol. 13 (1) (2018) JTST0012.

[29] K. Yue, X. Zhang, Y.Y. Zuo, Noninvasive method of simultaneously measuring the thermophysical properties and blood perfusion in cylindrically shaped living tissues, Cell Biochem. Biophys. 50 (2008) 41–51.